Computational Simulation of Temperature Elevations in Tumors Using Monte Carlo Method and Comparison to Experimental Measurements in Laser Photothermal Therapy

Navid Manuchehrabadi

Yonghui Chen

Alexander LeBrun

Ronghui Ma

Liang Zhu[1]

e-mail: zliang@umbc.edu

Department of Mechanical Engineering,
University of Maryland Baltimore County,
1000 Hilltop Circle,
Baltimore, MD 21250

Accurate simulation of temperature distribution in tumors induced by gold nanorods during laser photothermal therapy relies on precise measurements of thermal, optical, and physiological properties of the tumor with or without nanorods present. In this study, a computational Monte Carlo simulation algorithm is developed to simulate photon propagation in a spherical tumor to calculate laser energy absorption in the tumor and examine the effects of the absorption (μ_a) and scattering (μ_s) coefficients of tumors on the generated heating pattern in the tumor. The laser-generated energy deposition distribution is then incorporated into a 3D finite-element model of prostatic tumors embedded in a mouse body to simulate temperature elevations during laser photothermal therapy using gold nanorods. The simulated temperature elevations are compared with measured temperatures in PC3 prostatic tumors in our previous in vivo experimental studies to extract the optical properties of PC3 tumors containing different concentrations of gold nanorods. It has been shown that the total laser energy deposited in the tumor is dominated by μ_a, while both μ_a and μ_s shift the distribution of the energy deposition in the tumor. Three sets of μ_a and μ_s are extracted, representing the corresponding optical properties of PC3 tumors containing different concentrations of nanorods to laser irradiance at 808 nm wavelength. With the injection of 0.1 cc of a 250 optical density (OD) nanorod solution, the total laser energy absorption rate is increased by 30% from the case of injecting 0.1 cc of a 50 OD nanorod solution, and by 125% from the control case without nanorod injection. Based on the simulated temperature elevations in the tumor, it is likely that after heating for 15 min, permanent thermal damage occurs in the tumor injected with the 250 OD nanorod solution, while thermal damage to the control tumor and the one injected with the 50 OD nanorod solution may be incomplete.
[DOI: 10.1115/1.4025388]

Keywords: laser photothermal therapy, tumor optical properties, gold nanorods, Monte Carlo simulation, bioheat transfer modeling

Introduction

In recent years, laser photothermal therapy using gold nanoshells or gold nanorods has been tested as a hyperthermia approach due to its ability to deliver and confine adequate thermal dosage to tumors, which overcomes limitations of collateral thermal damage to superficial tissue in traditional laser therapy. Various studies [1–5] have demonstrated that the geometrical parameters of gold nanoshells or nanorods can be tuned to enhance laser absorption at a specific laser wavelength. The underlying mechanism is plasmon resonances of gold nanostructures when their sizes are much smaller than the visible light wavelength [6,7]. It has been suggested that the near infrared (NIR) laser with a wavelength of approximately 800 nm may penetrate into deep normal tissue with minimal laser absorption before reaching the target tumor containing gold nanoshells or nanorods [8]. Designing an optimal heating protocol in laser photothermal therapy may be performed using theoretical approaches to test effects of various parameters on the resulted temperature field. However, accurate simulation of temperature elevations in tumors relies on not only the laser power setting but also a precise description of thermal, optical, and physiological properties of tumors with or without nanorod deposition [9–12].

Various experiments have been conducted in the past several years to evaluate the effectiveness of laser photothermal therapy in cancer treatment both in tissue cultures and implanted tumors in mice [2, 4–6, 13–22]. Most in vivo experiments performed on mice involve injecting approximately 0.1–0.2 cc of nanoshell solutions (concentration varies from 10^9 to 10^{11} nanoshells per ml solution) into tumors. Typical laser irradiance at the surface is 2–50 W/cm^2 for the photothermal therapy to be effective [13,14,23,24]. Laser spot size, which is chosen to cover the tumor region laterally, varies from 1–5 mm [23,25]. Heating duration varies over a wide range. It can be shorter than several minutes or longer than 15 min [3,14,23]. Successful treatment outcomes are illustrated by shrinkage of tumors following the laser therapy, as well as observed tumor cell death in tissue culture.

Limitations of the previous studies include unknown temperature fields in the entire tumor during laser treatment. In most

[1]Corresponding author.

Contributed by the Bioengineering Division of ASME for publication in the JOURNAL OF BIOMECHANICAL ENGINEERING. Manuscript received May 31, 2013; final manuscript received August 27, 2013; accepted manuscript posted September 12, 2013; published online October 10, 2013. Assoc. Editor: Ram Devireddy.

experiments, only one or two locations are measured, without information on the temperatures at the tumor periphery. Other approaches, such as infrared thermography imaging, are only capable of measuring temperature profiles of the tumor surface [24]. In light of this, a computational simulation may give a detailed description of temperature distribution in the tumor and help obtain a better understating of the three-dimensional heat transfer in tumors during laser photothermal therapy.

Modeling laser-tissue interaction is beneficial for analyses and optimization of the parameters determining laser energy absorption. Traditionally, laser propagation in tissue can be simulated either based on the diffusion approximation solution approach considering the laser as a source term and the fluorescence effect of the laser beam [26] or based on stochastic analyses, accounting for the statistical uncertainty of laser propagation in tissue. One widely used stochastic analysis is Monte Carlo simulations in which the expected value of a certain random variable is determined by running multiple trial runs to yield statistical results [27]. Since it was first introduced [28], the Monte Carlo simulation has been extensively used to simulate light transport in media for various applications [29–37].

The Monte Carlo method, which is statistical in nature, simulates a "random walk" of a large number of photons in a medium that absorbs and scatters light [38]. It is considered a rigorous, accurate, and versatile method to give a reliable prediction of laser energy deposition [39]. A Monte Carlo simulation of light transport is based on macroscopic optical properties that are assumed to extend uniformly over small units of tissue volume. The simulation does not consider details of radiant energy distribution within the unit.

In a Monte Carlo simulation, laser irradiance on a surface is represented by emitting a large quantity of photons. Once a photon reaches the boundary surface, part of its weight will be specularly reflected before the rest moves across the boundary. It then undergoes a series of events of scatterings and absorptions, as shown in Fig. 1, and the final volumetric heat generation rate in tissue is determined by calculating the accumulated photon weight per unit tissue volume. The trajectory of a photon in tissue is determined by two key factors, the mean free path and the deflection angel for an absorption or scattering event. The rules of photon propagation are expressed as probability distributions for the incremental steps of photon movement between sites of photon-tissue interaction for the angles of deflection in a photon's trajectory when a scattering event occurs and for the probability of transmittance or reflectance at boundaries [40,41]. The Monte Carlo simulation requires information of the optical properties of the medium, which include the absorption coefficient (μ_a), the scattering coefficient (μ_s), and the anisotropic factor (g). Optical properties of tissues are typically determined by experimental measurements of excited tissue sample [42]. For example, μ_s and μ_a of liver tissue is 10 times bigger than that of prostate or breast tissue. Melanin in the skin and hemoglobin in the blood may greatly enhance these two coefficients [43,44]. The anisotropic factor is nearly constant ($0.9 \sim 0.97$) for most tissues. An anisotropic factor close to unity implies that most scattering events result in forwarding motion of photons, rather than being scattered back to the superficial layers of tissue. Since gold nanorod-induced photothermal therapy is a newly developed nanotechnology, none of the previous studies have quantified or measured optical properties of tumor containing the gold nanorods used in our previous studies [45].

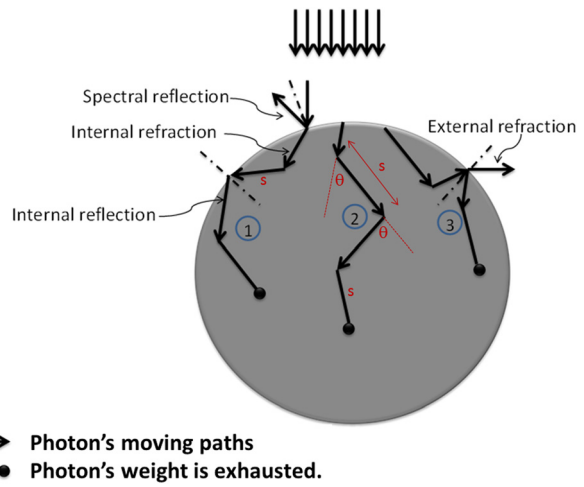

Fig. 1 Possible path trajectories for incident photons on the tumor top surface

Recent micro computed tomography (microCT) studies by our group have suggested that a gold nanorod solution injected into PC3 prostatic tumors results in an almost uniform distribution of the gold nanorods in the tumors [45]. Therefore, it is reasonable to assume that the nanorod-enhanced optical properties are uniform in the PC3 tumor. In this study, we would like to develop a computational algorithm of a Monte Carlo simulation of photon propagation in a spherical tumor containing gold nanorods to calculate laser energy deposition in tumors. The effects of μ_a and μ_s on the laser energy absorption in tumors will be examined. The laser energy absorption distribution will be imported to a 3D mouse model with spherical tumors implanted on its back to simulate three-dimensional heat transfer during laser photothermal therapy. The simulated temperature elevations in tumors will then be compared to our previous experimental measurements of tumor temperatures to extract the optical properties of PC3 tumors containing gold nanorods of different concentrations.

Materials and Methods

Monte Carlo Simulation. The Cartesian coordinate system is used in the Monte Carlo simulation to trace photon movements. The z-axis is parallel to the direction of the laser irradiation. Each photon is initially assigned a weight (W_0) based on the laser irradiance incident on the top surface of the tumor. After the initial partial specular reflection on the tumor top surface, the step size of the photon inside the tumor s is calculated based on sampling of the probability for the photon's free path $s(0,\infty)$. According to the definitions of the absorption coefficient and scattering coefficient, the step size is determined by

$$s = -(\ln \zeta)/(\mu_a + \mu_s) \tag{1}$$

where ζ is a random variable in (0,1]

After the photon moves a step size to its new location, attenuation of the photon weight due to absorption by the tissue must occur, depending on the absorption coefficient and scattering coefficient. The amount of deposited photon weight, ΔW_i at location i, is calculated by

$$\Delta W_i = W_i[\mu_a/(\mu_a + \mu_s)] \tag{2}$$

Note that ΔW_i is associated with the specific photon incident on the tumor surface and the tumor location. As it will be shown later, the deposited photon weights at each tumor location from all the photons incident on the tumor surface will be added together to represent laser energy absorbed by the tumor location per unit time (watt). The photon weight decreases from its previous value W_i to W_{i+1}

$$\begin{aligned} W_{i+1} &= W_i - \Delta W_i \\ &= W_i - W_i[\mu_a/(\mu_a + \mu_s)] \\ &= W_i[\mu_s/(\mu_a + \mu_s)] \quad i = 1, 2, 3, \ldots \end{aligned} \tag{3}$$

Before the photon moves to its next location, scattering occurs so that the trajectory of the photon is determined by a deflection angle θ and an azimuthal angle Ψ from its previous path direction. A widely used probability distribution of the cosine of the deflection angle is as,

$$f(\cos\theta) = \frac{1-g^2}{2(1+g^2-2g\cos\theta)^{3/2}} \tag{4}$$

Based on Eq. (4), the cosine of the deflection angle is determined by using a random variable ζ between (0,1]:

$$\cos\theta = \frac{1}{2g}\left[1+g^2-\left(\frac{1-g^2}{1-g+2g\zeta}\right)^2\right] \tag{5}$$

Ignoring the asymmetric scattering in azimuthal direction gives a constant probability density function and an azimuthal angle Ψ that is uniformly distributed within the interval [0, 2π], i.e., $\Psi = 2\pi\zeta$.

Therefore, as the photon moves from one location to the next in tissue, the absorption and scattering events occur and the photon weight decreases consequently. The propagation of the photon is terminated when the photon weight is lower than a threshold value of less than 0.1% of its initial value or when a photon is out of the computational domain. In order to get a statistically meaningful result, the trajectories of a large number of photons will be simulated and the accumulated photon weight is stored in grid elements to calculate the volumetric heat generation rate distribution.

Simulation Parameters. The Monte Carlo simulation is performed on a spherical tumor of 10 mm in diameter. As shown in Fig. 2, laser energy is incident on a projected circular surface of the tumor top surface with a spot size of 7 mm in diameter. In our previous studies [45], 0.1 cc of a gold nanorod solution was injected into the center of the tumor and it showed an almost uniform distribution of the nanorods in tumors after the intratumoral injection. Therefore, the tumor is modeled as one entity with uniform optical properties. In this study, the laser irradiance incident on the tumor surface is 1.6 W/cm^2. Since the incident surface is a circular area with a diameter equal to 7 mm, the total incident laser power can then be calculated as $I_0 = 0.615$ W. The incident surface on the tumor top surface is divided into N subsurfaces ($N = 952$). The total number of photons projected onto each subsurface N_0 is 200, with a total of 190,400 (N^*N_0) photons used, assuming that the laser irradiance is uniformly distributed on the tumor top surface. Since all the photons should have the same initial weight, the initial weight of each photon (watt) can then be calculated as

$$W_0 = I_0/(N_0 * N) \tag{6}$$

The tumor volume is then divided into cubic elements. As described earlier, the deposited photon weights ΔW in each cubic element from all 190,400 photons will be added together to calculate the total laser energy absorbed by that specific cubic element. The volumetric heat generation rate in the specific cubic element in the tumor in term of W/m^3 is then determined by dividing the deposited photon weight (watt) in the specific cubic element by the cubic element volume (m^3).

Since the Monte Carlo method is a stochastic approach, a large number of photons are needed to obtain statistically repeatable results. The total number of photons incident on each subsurface (N) is increased from 200 to 2000 to test the sensitivity. The numerical simulations suggest a very small difference (less than 1%) in the average specific absorption rate (SAR) value resulting from the increase in the number of photons. The tumor volume is divided into cubic elements ($0.2\times0.2\times0.2$ mm^3 in each element). We have tested the sensitivity of the element size by increasing the number of the elements by 400% and found that it results in a difference of 1% difference in the average tumor temperature.

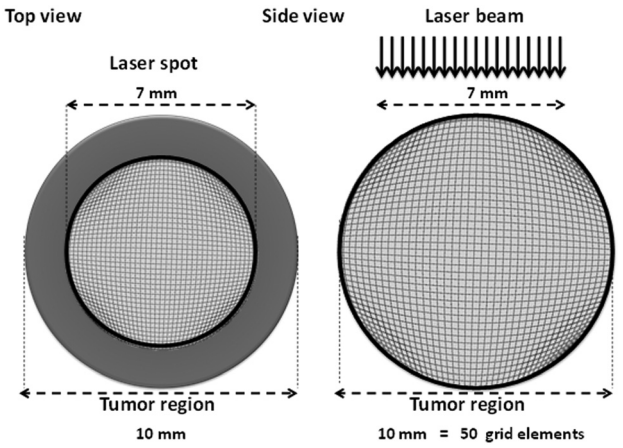

Fig. 2 The left panel shows the subregions of the top surface of a spherical tumor irradiated by a laser spot of 7 mm in diameter. The right panel illustrates individual grid elements which are 0.2 × 0.2 × 0.2 mm^3 in volume in the tumor region.

Generation of a Mouse Model. A BALB/c Nu/Nu male mouse from an albino laboratory-bred strain of the house mouse (National Cancer Center, 3 months old) was scanned in a microCT imaging system (Skyscan1173, MicroPhotonics, PA) to obtain the geometry of the mouse model (Fig. 3). Due to the memory limitation of our computer, the mouse model was reconstructed based on 15 digital slices of the CT scans using ProE software. The ProE file representing the mouse geometry was then imported into COMSOL® 4.3 Multiphysics software package via the LiveLink™ interface.

Heat Transfer Model in COMSOL®. The temperature elevation in prostate tumors was modeled using COMSOL® Multiphysics 4.3. Figure 3 depicts the computational domain for modeling laser photothermal therapy in COMSOL® with two tumors implanted on the flanks. The two tumors are implanted into the mouse model with 1/4 of the tumors inside the mouse body. To mimic the experimental settings in our previous study, only one of the tumors is heated using the 808 nm laser incident on the top surface of the tumor.

The Pennes bioheat equation is used to simulate the steady state temperature fields of the tumors and the mouse body [46]. They are written as

$$\text{Mouse body } 0 = k_{\text{tissue}}\nabla^2 T_{\text{tissue}} + \omega\rho_b c_b(T_b - T_{\text{tissue}}) + Q_{\text{met,tissue}} \tag{7}$$

$$\text{Tumor } 0 = k_{\text{tumor}}\nabla^2 T_{\text{tumor}} + \omega\rho_b c_b(T_b - T_{\text{tumor}}) + Q_{\text{met,tumor}} + Q_{\text{laser}} \tag{8}$$

where T_{tissue} is mouse tissue temperature, T_{tumor} is tumor temperature, T_b is the temperature of the arterial blood and it is equal to 37 °C, k_t is thermal conductivity of tissue, ρ_b is blood density, c_b is specific heat of blood, and Q_{met} is metabolic heat generation rate. Note that the specific absorption rate (SAR), represented by Q_{laser} in Eq. (8), is calculated from the Monte Carlo simulation and is only applied to the tumor subject to laser irradiance. The bottom surface of the mouse body is assumed to be at a constant temperature equal to that of a heating pad at 37 °C. All the other lateral surfaces are assumed to exchange heat with the surrounding air ($T_{\text{air}} = 20$ °C) by convection. The overall heat transfer coefficient (h) accounting for both natural heat convection and radiation was calculated to be approximately 10 W/m^2 °C.

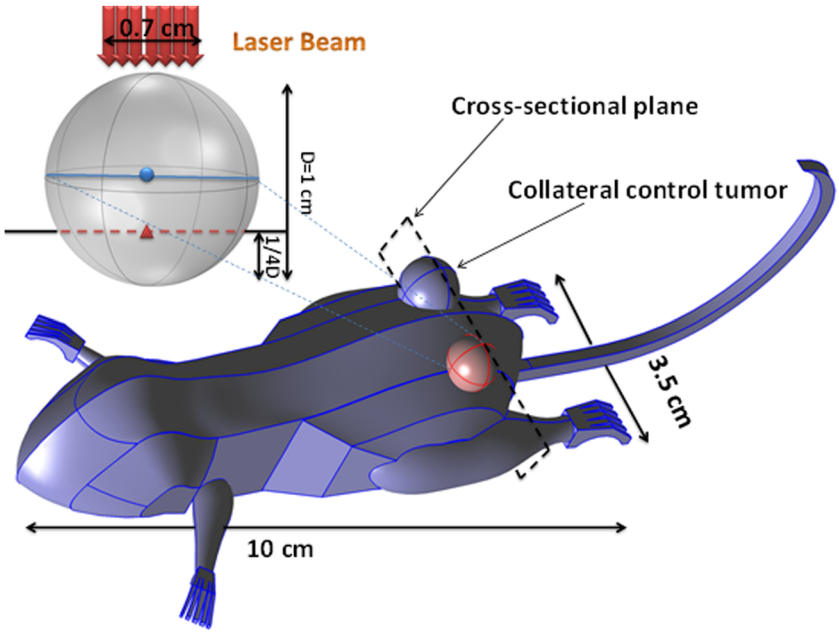

Fig. 3 The generated mouse model and the two embedded tumors. The thermocouple paths are illustrated in the spherical tumor as solid and dash lines.

The computations were conducted using LiveLink™ COMSOL® 4.3 for finite element simulation of the temperature distribution. The total quadratic tetrahedral elements in the three-dimensional mouse model is 31,362 with a total number of degree of freedom of 74,286. We have tested the sensitivity of the mesh size by increasing the total number of the elements by 50% and found that it resulted in a difference of less than 1% in the average tumor temperature.

Extraction of the Optical Properties. Previous experiments have been performed by our group to obtain temperature elevations in PC3 tumors during laser photothermal therapy [45]. The details of the experiment can be found in our previous publication. Briefly, after the injection of 0.1 cc of a 250 OD gold nanorod solution (2.1×10^{14} nanoparticles per ml (NPS/ml)) into one of the tumors, two fine copper-constantan thermocouples with a wire diameter of 100 μm were inserted into the tumor to map the temperature elevations in the tumor. In order to place the thermocouple in the tumor, a 22-gauge needle was inserted first and went through the center of the spherical tumor all the way to the other end. The thermocouple was inserted into the needle from one side until it reached the other side. Then, the needle was pull out of the tumor. The second thermocouple was fixed with the same procedures except that it passed the center of the bottom surface of the tumor, which was the interface between the tumor and the mouse body. Then, the tumor was subject to laser heating using a Ti:Sapphire laser at 808 nm incident on the top surface of the tumor. The laser radiance at the tumor surface was fixed at 1.6 W/cm^2 (an average power of 0.6 W and a laser spot of 7 mm in diameter). After steady state, the thermocouples were pulled to map the steady state temperatures along the two tumor paths. The recorded temperatures at various locations in the tumor will be used for extracting optical properties in the PC3 tumors with the 250 OD nanorod injection. Similar experiments were performed on implanted PC3 tumors without nanorod injection or in tumors injected by 0.1 cc of a 50 OD nanorod solution. The 50 OD nanorod solution (3.2×10^{13} NPS/ml) is less concentrated than the 250 OD nanorod solution.

Compared to the obtained experimental temperature measurements inside the laser irradiated tumor, an inverse heat transfer analysis was applied to extract the optical properties (μ_a and μ_s) of the prostatic tumors without or with the gold nanorods to the 808 nm laser. The SAR distribution was calculated via the developed computational algorithm of the Monte Carlo simulation of photon propagation in a spherical tumor with nanorods, as shown in the section of Monte Carlo Simulation. Then the SAR file was imported to the tumor region to simulate the temperature fields of the tumor and the mouse body. An objective function based on the least square residual fit is defined by the following expression:

$$\mathrm{LSQ}(\mu_a, \mu_s) = \frac{\sqrt{\sum_{i=1}^{M} [\Phi_i - T_i(\mu_a, \mu_s)]^2}}{M} \tag{9}$$

where M is the total number of the measured temperatures along the two tumor paths, Φ_i and T_i represent the experimentally measured and theoretically predicted temperatures, respectively, at individual tumor locations. The experimental values used in Eq. (9) are the average temperatures of all the tumors studied. The values of the absorption and scattering coefficients were adjusted until the objective function reaches its minimal. The obtained absorption and scattering coefficients then represent the optical properties of the tumors with or without nanorod depositions.

Results

Table 1 gives a summary of laser parameters for the Monte Carlo simulation. The anisotropic factor g is assumed equal to 0.9 [39]. The spectral reflectivity at the tumor surface is calculated as 0.0298 [41], representing less than 3% of the initial photon weight. The simulation is carried out so that both μ_a and μ_s vary within large ranges due to the uncertainty of the optical properties. The size of the tumor has a volume similar to the average tumor volume measured in our previous experimental studies (691 ± 62 mm^3) [45].

The four panels in Fig. 4 demonstrate how the absorption coefficient affects the laser energy absorption distribution in the tumor. The tapered SAR pattern in the tumor is largely due to the concave shape of the tumor top surface where the laser is incident. Although scattering is considered in the model ($\mu_s = 1.5\,\mathrm{cm}^{-1}$), laser energy absorption outside of the dominant absorption region is minimal. The percentage shown at the bottom right corner in each panel gives the total percentage of the laser energy absorbed

Table 1 Summary of the laser simulation variables

Anisotropic factor	Scattering coefficient	Absorption coefficient	Laser irradiance	Laser power	Reflectivity
g	μ_s (cm^{-1})	μ_a (cm^{-1})	I_0 (W/cm^2)	P (W)	r
0.9	0–30	0.5–3	1.6	0.6	0.0298

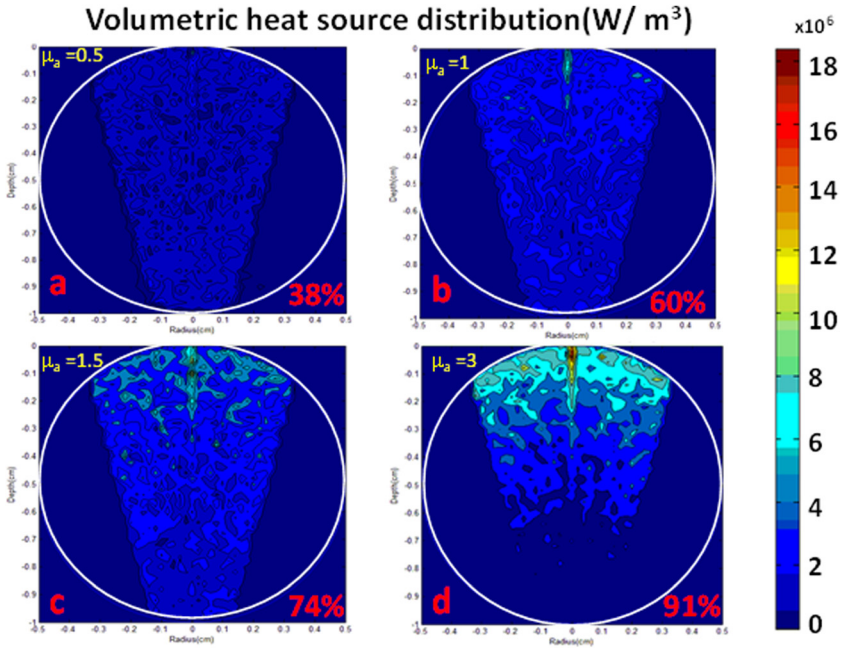

Fig. 4 The effect of the absorption coefficient on the SAR distribution in the spherical tumor while the scattering coefficient μ_s is kept unchanged as 3 cm^{-1}

by the tumor. Increasing the absorption coefficient greatly enhances the total laser energy absorption by the tumor. The rest of the laser energy is either specularly reflected on the tumor top surface (2.98%), or it escapes from the tumor surface before its energy is exhausted (59%–6%). The energy absorption increases monotonously with μ_a until it almost saturates when μ_a exceeds 3 cm^{-1}, with only 6% of the laser energy escaping from the tumor surface. On the other side, a continuous increase in the absorption coefficient higher than 3 cm^{-1} may shift the distribution of laser deposition in the tumor; however, it is a waste of the resource of nanorods since the majority of the laser energy has been confined in the tumor.

The effect of the scattering coefficient on the SAR distribution is presented in Fig. 5 where the absorption coefficient is kept unchanged as 1.5 cm^{-1}. The scattering coefficient μ_s varies from no scattering (0 cm^{-1}) to significant scattering (30 cm^{-1}). Clearly with an increase in the scattering effect, the step size of individual photons in the tissue will be greatly shortened, resulting in diminishing chance of the photons to escape from the tumor domain. The major contribution of the enhanced scattering coefficient is to shift most of the laser energy to the top region of the tumor. Among all the laser energy escaping from the tumor surface, a larger μ_s results in most of the laser energy escaping from the upper hemispherical tumor surface rather than from the lower tumor surface. Surprisingly, the scattering coefficient has a minor effect on the percentage of the total laser energy absorbed by the tumor, at approximately 74% over the range of the scattering coefficient when the absorption coefficient is 1.5 cm^{-1}.

The physical parameters and thermal properties of the mouse tissue and tumor prostate used in the numerical simulation from literature are given in Table 2. The thermal and physiological properties of tissue have been reported in the literature [39,47–49]. It is not clear how the blood perfusion rate in the tumor changes during the heating. Previous experiments using the same heating protocol [45,50] on PC3 tumors have demonstrated permanent thermal damage to the tumors; therefore, it is reasonable to assume that the blood supply to the tumors after 15 min of laser heating may have ceased when the tumor temperatures were recorded. In Table 2, the tumor blood perfusion rate and the metabolic heat generation rate are, therefore, selected as zero. For the 250 OD case, 63 sets of μ_s and μ_a are tested to obtain temperature distributions in the tumor. The least square residual fit is preformed to calculate the difference between the experimental and theoretical temperature distribution in the laser irradiated tumor. Figure 6 gives the obtained objective functions for different combinations of the absorption and scattering coefficients. As shown in Fig. 6, the objective function is the smallest when $\mu_a = 1.1$ cm^{-1} and $\mu_s = 7$ cm^{-1}, which represent possible optical coefficients of the PC3 tumors injected by 0.1 cc of the 250 OD gold nanorod solution. Table 3 gives the three sets of the extracted μ_s and μ_a for the three cases. Both μ_s and μ_a are higher in tumors containing more nanorods. In the tumor tissue without nanorods present, the absorption coefficient is 37% of that of the tumors injected by 0.1 cc of the 250 OD gold nanorod solution.

The theoretical and experimental tumor temperature distributions during laser photothermal therapy are shown in Fig. 7 when using the fitted optical properties of the tumor injected with the 250 OD nanorod solution. The two paths for the temperature mappings in the tumor are also illustrated on the right bottom of the figure. The theoretical temperature predictions agree reasonably well with the experimental measurements, having an average deviation of less than 0.7 °C.

Since the experimental study only records temperatures at limited locations in the tumor, the theoretical simulation is used to

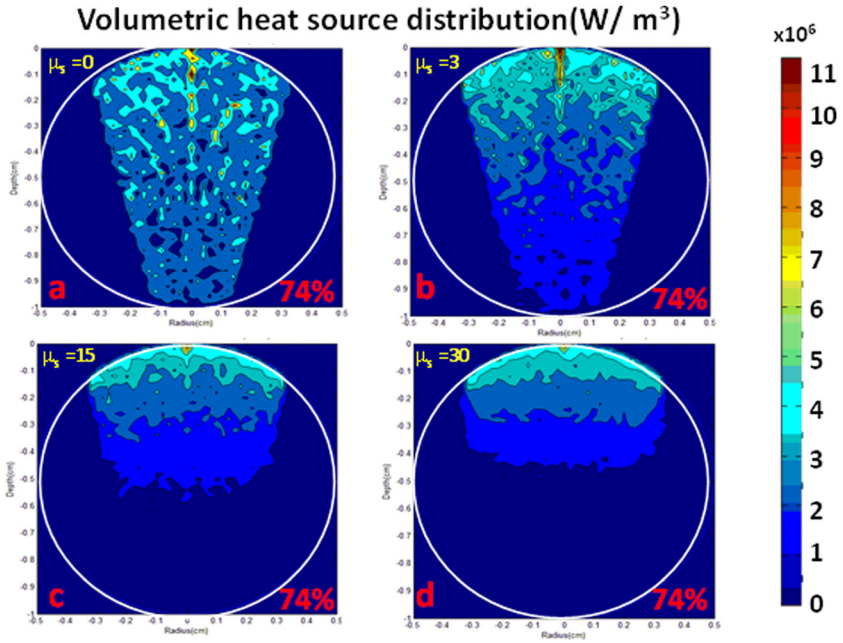

Fig. 5 The effect of the scattering coefficient on the SAR distribution in the spherical tumor while the absorption coefficient μ_a is kept unchanged as 1.5 cm^{-1}

Table 2 Thermal and physiological properties obtained from the literature [39,47–49]

	ω (s^{-1})	Q_{met} (W/m^3)	ρ_b (kg/m^3)	k (W/mK)	c_b (J/kgK)
Tumor	0	0	1060	0.5	3960
Mouse tissue	0.00018	450	1060	0.5	3960

give a complete temperature field in the tumor. The SAR distribution generated from the Monte Carlo simulation ($\mu_a = 1.1$ cm^{-1} and $\mu_s = 7$ cm^{-1}) for the 250 OD case is depicted in Fig. 8(*a*). Figure 8(*b*) shows the enlarged SAR contour map in the mouse model, while the top view of the SAR distribution is illustrated in Fig. 8(*c*). Using the fitted optical properties, the average SAR induced by laser irradiance is 8.5×10^5 W/m^3 in the tumor, while the volumetric heat generation rate in the mouse body is caused only by local metabolism and blood perfusion effects. Table 4 shows how the laser energy is conserved using the Monte Carlo simulation. As expected, only 35% of the laser energy is confined in the tumor without nanorods, while it increases to 67% in the tumor injected with the 250 OD nanorod solution. Since the tumor is protruding from the mouse back, one sees significant laser energy escaping from the tumor surface, especially from the bottom half of the spherical surface (30–60%). The last column

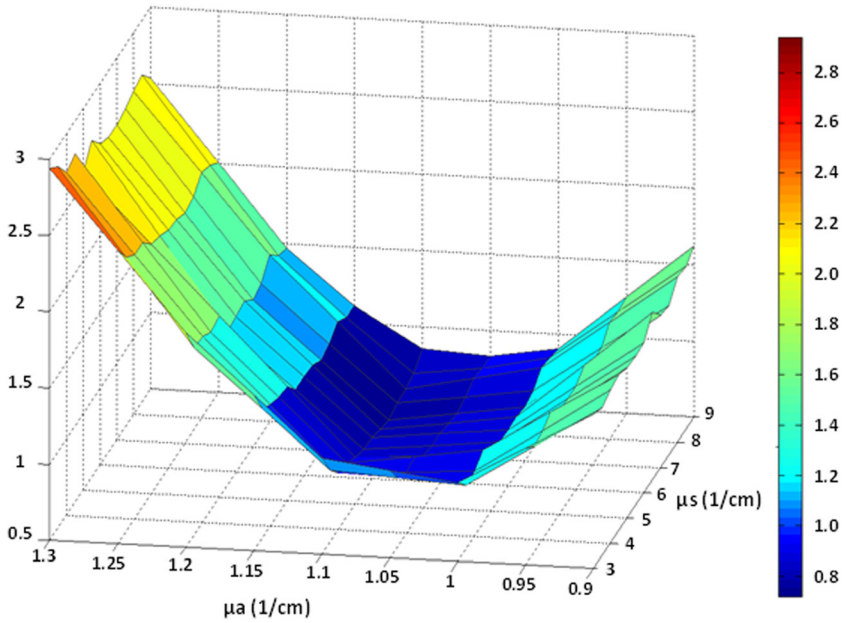

Fig. 6 The obtained objective function values for various combinations of the absorption and scattering coefficients in the 250 OD injection case. The objective function is the smallest when $\mu_a = 1.1$ cm^{-1} and $\mu_s = 7$ cm^{-1}.

Table 3 Extracted scattering coefficient μ_s and absorption coefficient μ_a of the PC3 tumors containing different nanorod concentrations

	μ_s (cm^{-1})	μ_a (cm^{-1})	μ_s/μ_a
Without nanorod injection	5	0.41	12.19
Injection of 0.1 cc of 50 OD gold nanorod solution	6	0.8	7.5
Injection of 0.1 cc of 250 OD gold nanorod solution	7	1.1	6.36

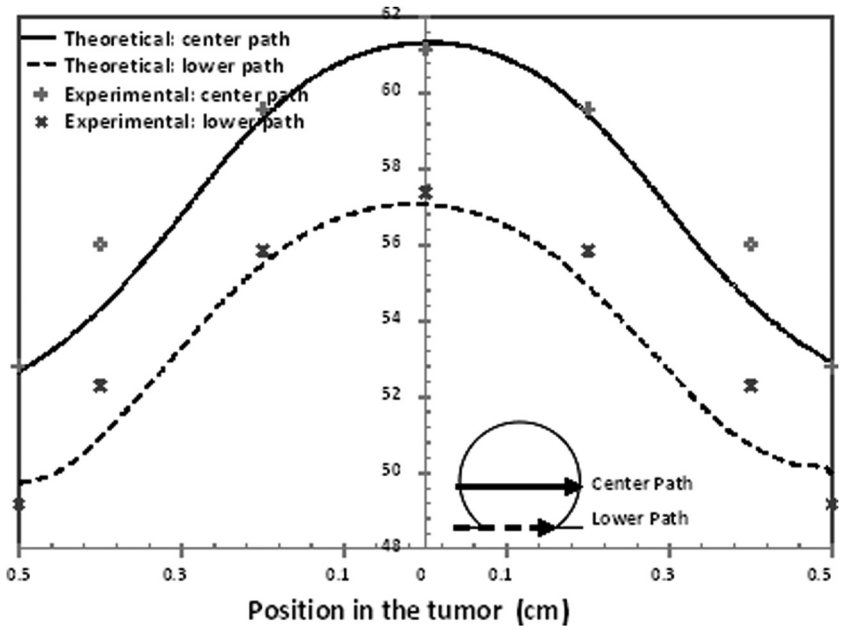

Fig. 7 Experimental (symbols) and theoretical (lines) temperature distribution profiles in the tumors during laser photothermal therapy in the 250 OD injection case. Temperature mappings are along two tumor paths shown on the right bottom of the figure.

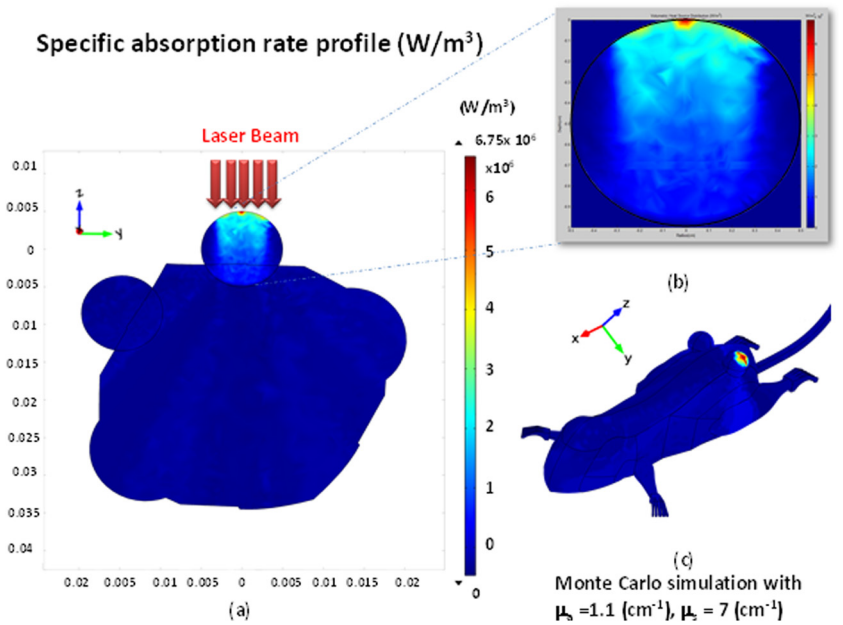

Fig. 8 Panel (*a*) gives the SAR contour map along the centerline in the mouse model, including the mouse body and the tumor. An enlarged SAR distribution in the tumor in the 250 OD injection case is shown in panel (*b*). The top view of the SAR distribution in the 3D structure of the mouse model is illustrated in panel (*c*).

Table 4 Energy conservation in the Monte Carlo simulations for the three cases

Cases	Specularly reflected energy	Absorbed by the tumor	Escaping from the bottom hemispheric surface	Escaping from the top hemispheric surface	Total
No nanorod	2.98%	35.52%	51.71%	8.97%	99.2%
50 OD	2.98%	55.50%	33.87%	6.92%	99.3%
250 OD	2.98%	66.08%	24.26%	6.02%	99.4%

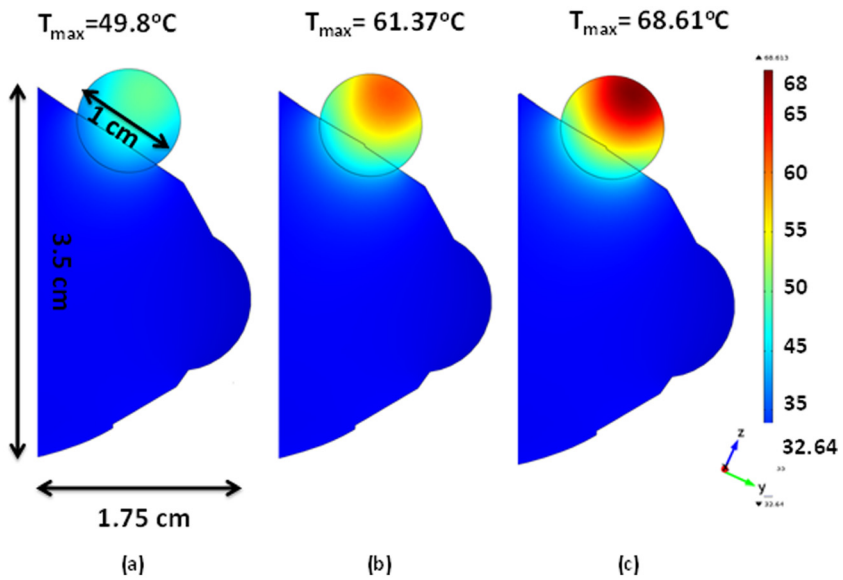

Fig. 9 The temperature contours inside the tumor based on the obtained optical properties of the tumor. (*a*) No nanorod injection, (*b*) the tumor is injected with 0.1 cc of the 50 OD nanorod solution, and (*c*) the tumor is injected with 0.1 cc of the 250 OD nanorod solution.

shows laser energy conservation in the Monte Carlo simulation results.

The resulting temperature fields in the tumor for the three cases during laser photothermal therapy are presented in Fig. 9. The laser irradiance has a very minor effect on the temperature field of the mouse body, which has a relatively uniform temperature distribution. With the heat generated in the tumor in the 250 OD case, the tumor temperature is elevated significantly from its baseline of 37 °C, varying from 47 °C on the bottom of the tumor to 68 °C on the top surface irradiated by the laser. Due to the laser penetration in the tumor, the maximal temperature of 68 °C is located 1 mm below the top surface, while the temperature at the tumor center is approximately 61 °C. On the other hand, the maximal temperature of the tumor without nanorod injection is only 49.7 °C, located 2.1 mm below the top surface. 39 °C is the temperature at the tumor bottom surface without nanorod injection. In general, temperatures are lower in the tumor periphery than in the tumor central region. The nonuniform temperature distribution of the tumor temperature field again emphasizes the challenge faced by clinicians to induce uniform thermal damage to the entire tumor.

Discussion

Laser photothermal therapy has the potential for treating local prostatic tumors. For prostatic cancer treatment, regional hyperthermia has been considered minimally invasive due to transurethral or transrectal access to the prostate. Temperature elevations in tumors can be achieved via laser energy emitted from a laser catheter inserted in the prostatic urethra. In addition, cooling using cold water circulating inside the catheter may be implemented to protect the sensitive prostatic urethra. Utilizing near-infrared laser at 800 nm in wavelength provides an advantage to minimize laser energy absorption by prostatic tissue near the prostatic urethra, therefore, maximizing heat absorption by the tumor with nanorods. This goal can be achieved by carefully designing heating protocols via theoretical simulations before the actual laser treatment. The predictive power of theoretical simulations relies on accurate measurements of thermal and optical properties of tumor tissue with or without nanorods present.

The Monte Carlo simulation allows calculation of reflection, transmission, and absorption of photon weight in tissue. Our previous experimental studies have shown that the gold nanorods used in our study are almost uniformly distributed in the prostatic tumors after intratumoral injections. Therefore, the optical properties of the tumors can be assumed uniform in the calculation domain. However, the distribution of nanostructures may not always be isotropic as in this study. It is not clear whether other kinds of nanorods or nanoshells having different sizes and/or shapes will result in the same deposition patterns as in our study. In a systemic delivery, it is even more unpredictable since the nanostructure distribution in tumors depends on not only local blood perfusion rate but also permeability of the vasculature and coating on the nanostructures. Therefore, other image techniques are needed to understand the possible heterogeneous distribution of the optical properties in tumors for precise simulation using the Monte Carlo method.

We have demonstrated the impact of absorption and scattering coefficients on the thermal energy absorption in tissue. Typically, a tissue region having both absorption and scattering cannot be described by Beer's law, which states that the laser absorption is one-dimensional and laser irradiance decays following an

exponential function. Previous studies have proposed an expression similar to Beer's law via combining the absorption and scattering together, leading to a definition of the effective attenuation coefficient [27,28]

$$\mu_{\text{eff}} = \mu_a + (1-g)\mu_s \tag{10}$$

Therefore, Beer's law can still be used except that the absorption coefficient in Beer's law is replaced by the effective attenuation coefficient μ_{eff}. Based on this expression, the role played by scattering is equivalent to an enhancement in absorption, while the anisotropic factor g is considered as a factor that diminishes the scattering effect when g is positive. Examining our simulation following photons' propagation in the tissue region, our model can be used to assess whether Eq. (10) reasonably represents propagation and absorption in the PC3 tumors used in our studies. One finds that the energy absorbed deviates significantly from the simple one-dimensional propagation and a majority of photon energy may escape from the tumor surfaces, especially when scattering is strong. Our result also illustrates that an increase in the scattering coefficient has very little influence on the total laser energy absorbed by the tissue region, unlike that predicted by Eq. (10). It is possible that Eq. (10) may still be a reasonable estimation of laser energy absorption if the considered domain is an infinite plane perpendicular to the laser incident direction. Therefore, Eq. (10) may still be valid under certain circumstances. However, it would have led to inaccuracy if it were used to describe photon propagation in the spherical structure described in this study.

Since laser photothermal therapy is a newly developed technique in recent years, investigation of optical properties enhanced by the presence of nanostructures is limited. Our study has attempted to extract optical properties of PC3 tumors injected by 0.1 cc of either 50 OD or 250 OD nanorod solution, as well as that of tumors without nanorod injection, using inverse heat transfer analyses. The range of the obtained optical properties agrees in general with several previous measurements by other groups. It has been shown [51] that the extinction coefficient of nanorods with transversal and longitudinal diameters of $13\,\text{nm} \times 47\,\text{nm}$ is dominated by absorption. This is in agreement with our Monte Carlo simulation that the total laser absorption rate by the tumor is more sensitive to the change of the absorption coefficient than that of the scattering coefficient. Our results ($\mu_a = 0.41\,\text{cm}^{-1}$ and $\mu_s = 7\,\text{cm}^{-1}$) agree very well with several previous results of prostatic tissue without nanorod injections. In Piao et al. it is reported that the absorption coefficient as $0.34\,\text{cm}^{-1}$ and the scattering coefficient varying from 0.25 to $1\,\text{cm}^{-1}$ for normal human prostate tissue to laser at 830 nm wavelength [43]. The measured absorption coefficients at 789 nm wavelength laser in prostatic tumor samples (R3327at) is $0.6 \pm 0.3\,\text{cm}^{-1}$, which is close to what is determined in our study in tumors without nanorod injection [52]. It is evident from previous studies that adding nanoshells or nanorods increases the absorption and scattering coefficients in tissue. Using a laser at 808 nm, gold nanoshell-enhanced thermal deposition was studied by Feng et al. [39]. The extracted absorption and scattering coefficients are $2.15\,\text{cm}^{-1}$ and $14.2\,\text{cm}^{-1}$, respectively [39]. Another study reported that the absorption coefficient of PC3 tumors in the presence of nanorods is $3.07\,\text{cm}^{-1}$ based on nanorod biodistribution and in vitro measurements [51]. In our study, the extracted absorption and scattering coefficients of the tumors injected with 0.1 cc of 50 OD gold nanorod solution to laser at 808 nm are 0.8 and $6\,\text{cm}^{-1}$, respectively. When the tumor is injected with 0.1 cc of a highly concentrated nanorod solution (250 OD), the extracted absorption coefficient of $1.1\,\text{cm}^{-1}$ is still smaller than that of the previous studies. The deviations among different studies may be due to variations of nanorod/nanoshell types and sizes and porous structures of tumors. Most importantly, the concentration of the injected nanorod solutions influences the optical property enhancements in PC3 tumors.

One limitation of the theoretical simulation is the uncertainty of the local blood perfusion rate and the responses of the blood flow to heating. Typically, the normal response of tissue to heating is to increase the local blood perfusion rate, as shown by previous studies [53,54]. However, the responses are more unpredictable in tumors. In this study, we assume that the vasculature of the tumors is damaged during the laser photothermal therapy; therefore, it is reasonable to assume that both the tumor blood perfusion rate and metabolism are zero. With blood supply to tissue, local metabolic heat generation rate is typically one or two orders of magnitude smaller than the heat generation rate by external devices such as laser, microwave, etc. However, the local blood perfusion rate, if it is sufficient, would act as a heat sink to carry away the heat, and it may have an order of magnitude similar to that of the heat generation rate by external devices [54]. It is always difficult to assess local blood perfusion rate without real-time simultaneous measurements of tumor temperatures and blood flow rates. Magnetic resonance imaging (MRI) may be a suitable way to measure them simultaneously.

Another limitation of the current work is the assumption of a spherical shape of the tumor. It will impose a challenge to implement Monte Carlo simulation if a tumor is irregular in shape. It is also difficult to embed a tumor with an irregular shape in the imported 3D mouse body in the COMSOL® software due to limitations of computational memory and difficulty in meshing. In the current study, the laser equipment used does not allow change in the laser parameters. It is important to point out that the laser beam size, laser power setting, and using a single- or multiple-beam delivery system will result in different energy deposition patterns desirable for target tissue. Future studies are warranted to continue to improve the computational algorithms so that the generated tumor geometry can be accepted by commercial finite element software packages for heat transfer simulations.

The computer model developed in this study is capable of predicting laser-induced temperature elevations in a prostate tumor by incorporating optical enhancements in the absorption and scattering coefficients due to the presence of gold nanorods. The Arrhenius integral [55] can be used to quantitatively assess thermal damage based on measured or simulated temperature history at various tissue locations. The obtained temperature contours in the entire tumor have illustrated that the minimal temperature in the tumor injected with 0.1 cc of 250 OD nanorod solution is still larger than 47 °C. Incorporating this temperature and the 15 min of heating time into the Arrhenius integral, one can assess thermal damage to the entire tumor. Using the same heating protocol, the occurrence of irreversible thermal damage in the entire tumor has been confirmed by the histological results and tumor shrinkage studies by our group [50]. However, without nanorod injection into the tumor, the minimal temperature of the tumor is barely 39 °C, thus it is unlikely that a heating duration of 15 min is sufficient to induced permanent thermal damage to some regions of the tumor with only several degrees above 37 °C. Injecting 0.1 cc of a 50 OD nanorod solution almost doubles the absorption coefficient from the $0.41\,\text{cm}^{-1}$ in the control case to $0.8\,\text{cm}^{-1}$, resulting in 56% more laser energy confined in the tumor than that in the control case. However, the minimal temperature in tumors injected by 0.1 cc of a 50 OD nanorod solution is only 44 °C, and it is unlikely to induce permanent thermal damage in the entire tumor when the heating duration is only 15 min. Nevertheless, the current study determines optical properties of tumor tissue with nanorods present, and it is the first step leading to predicting 3D temperature elevation contours in the entire tumor to assess thermal damage following a designed heating protocol.

In summary, a computational Monte Carlo simulation algorithm is developed to simulate photon propagation in a spherical tumor to examine the effects of the absorption and scattering coefficients of PC3 tumors on the generated heating pattern in spherical tumors. The laser-generated energy deposition distribution is then incorporated into a 3D finite-element model of a mouse body with prostatic tumors implanted on its flanks to simulate temperature

elevations during laser photothermal therapy using gold nanorods. The simulated temperature elevations are compared with experimentally measured temperatures in our previous in vivo experiment in PC3 prostatic tumors to extract the optical properties of the PC3 tumors containing gold nanorods of different concentrations. Our study has shown that the total laser energy deposited in the tumor is dominated by μ_a, while both μ_a and μ_s shift the distribution of the energy deposition in the tumor. Three sets of μ_a and μ_s are extracted, representing optical properties of PC3 tumors containing different concentrations of nanorods to laser irradiance at 808 nm wavelength. With the injection of 0.1 cc of the 250 OD gold nanorod solution, the total laser energy absorption rate is increased by 30% from the case of injecting 0.1 cc of the 50 OD nanorod solution and by 125% from the control case without nanorod injection. Based on the simulated temperature elevations in the tumor, it is likely that permanent thermal damage occurs in the tumor injected with the 250 OD nanorod solution when the heating time is 15 min, while thermal damage to the control tumor and the one injected with the 50 OD nanorod solution may be incomplete.

Acknowledgment

This research was supported in part by National Science Foundation Grants CBET-0821236 and CBET-1335958 and a research grant from UMBC Research Seed Fund Initiative. The research is performed in partial fulfillment of the requirements for the Ph.D. degree from the University of Maryland Baltimore County by Navid Manuchehrabadi.

References

[1] Bernardi, R. J., Lowery, A. R., Thompson, P. A., Blaney, S. M., and West, J. L., 2008, "Immunonanoshells for Targeted Photothermal Ablation in Medullo-Blastoma and Glioma: An In Vitro Evaluation Using Human Cell Lines," J. Neuro-Oncol., **86**(2), pp. 165–172.
[2] Gobin, A. M., Moon, J. J., and West, J. L., 2008, "Ephrin Al-Targeted Nano-Shells for Photothermal Ablation of Prostate Cancer Cells," Int. J. Nanomed., **3**(3), pp. 351–358.
[3] Melancon, M. P., Lu, W., Yang, Z., Zhang, R., Cheng, Z., Elliot, A. M., Stafford, J., Olson, T., Zhang, J. Z., and Li, C., 2008, "In Vitro and In Vivo Targeting of Hollow Gold Nanoshells Directed at Epidermal Growth Factor Receptor for Photothermal Ablation Therapy," Mol. Cancer Ther., **7**(6), pp. 1730–1739.
[4] Loo, C. H., Hirsch, L., Lee, M. H., Chang, E., West, J., Halas, N., and Drezek, R., 2005, "Gold Nanoshell Bioconjugates for Molecular Imaging in Living Cells," Opt. Lett., **30**, pp. 1012–1014.
[5] Loo, C. L., Lowery, A., Halas, N., West, J., and Drezek, R., 2005, "Immunotargeted Nanoshells for Integrated Cancer Imaging and Therapy," Nano Lett., **5**, pp. 709–711.
[6] Lal, S., Clare, S. E., and Halas, N. J., 2008, "Nanoshell-Enabled Photothermal Cancer Therapy: Impending Clinical Impact," Acc. Chem. Res., **41**(12), pp. 1842–1851.
[7] Skrabalak, S. E., Chen, J., Lu, X., Li, X., and Xia, Y., 2007, "Gold Nanocages for Biomedical Applications," Adv. Mater., **19**, pp. 3177–3184.
[8] Reidenbach, H.-D., 2007, "Laser Safety," *Springer Handbook of Laser and Optics*, F. Traeger, ed., Springer, New York.
[9] Mohammed, Y., and Verhey, J. F., 2005, "A Finite Element Method Model to Simulate Laser Interstitial Thermo Therapy in Anatomical Inhomogenous Regions," Biomed. Eng. Online, **4**(2), pp. 10–45.
[10] Welch, A. J., and van Gemert, M. J. C., 1995, "Optical-Thermal Response of Laser-Irradiated Tissue," A. J. Welch and M. J. C. van Gemert, eds., Plenum Press, New York.
[11] Engin, K., 1994, "Biological Rationale for Hyperthermia in Cancer Treatment (II)," Neoplasma, **41**(5), pp. 277–283.
[12] Dewhirst, M. V., Vujaskovic, Z., Jones, E., and Thrall, D., 2005, "Resetting the Biologic Rationale for Thermal Therapy," Int. J. Hypotherm., **21**(8), pp. 779–790.
[13] El-Sayed, I. H., Huang, X., and El-Sayed, M. A., 2006, "Selective Laser Photo Thermal Therapy of Epithelial Carcinoma Using Anti-EGFR Antibody Conjugated Gold Nanoparticles," Cancer Lett., **239**, pp. 129–135.
[14] O'Neal, D. P., Hirsch, L. R., Halas, N. J., Payne, J. D., and West, J. L., 2004, "Photo Thermal Tumor Ablation in Mice Using Near Infrared-Absorbing Nanoparticles," Cancer Lett., **209**, pp. 171–176.
[15] Xie, H., Gill-Sharp, K. L., and O'Neal, D. P., 2007, "Quantitative Estimation of Gold Nanoshell Concentrations in Whole Blood Using Dynamic Light Scattering," Nanomed Nanotech. Biol. Med., **3**, pp. 89–94.
[16] Weissleder, R., 2001, "A Clearer Vision for In Vivo Imaging," Nat. Biotechnol., **19**(4), pp. 316–317.
[17] Huang, X. W., Jain, P. K., El-Sayed, I. H., and El-Sayed, M. A., 2008, "Plasmonic Photothermal Therapy (PPTT) Using Gold Nanoparticles," Lasers Med. Sci., **23**, pp. 217–228.
[18] Ballou, B. L., Lagerholm, C., Ernst, L. A., Bruchez, M. P., and Waggoner, A. S., 2004, "Non-Invasive Imaging of Quantum Dots in Mice," Bioconjug. Chem., **15**, pp. 79–86.
[19] Choi, M. R., Stanton-Maxey, K. J., Stanley, J. K., Levin, C. S., Bardhan, R., Akin, D., Badve, S., Sturgis, J., Robinson, J. P., Bashir, R., Halas, N. J., and Clare, S. E., 2007, "A Cellular Trojan Horse for Delivery of Therapeutic Nanoparticles into Tumors," Nano Lett., **7**, pp. 3759–3765.
[20] Khlebtsov, B. N., Zharov, V., Melnikov, A., Tuchin, V., and Khlebtsov, N., 2006, "Optical Amplification of Photothermal Therapy With Gold Nanoparticles and Nanoclusters," Nanotechnology, **17**, pp. 5167–5179.
[21] Stern, J. M., Stanfield, J., Kabbani, W., Hsieh, J. T., and Cadeddu, J. A., 2008, "Selective Prostate Cancer Thermal Ablation With Laser Activated Gold Nanoshells," J. Urol., **179**, pp. 748–753.
[22] Krag, D. N., Fuller, S. P., Oligino, L., Pero, S. C., Weaver, D. L., Soden, A. L., Hebert, C., Mills, S., Liu, C., and Peterson, D., 2002, "Phage-Displayed Random Peptide Libraries in Mice: Toxicity After Serial Panning," Cancer Chemother. Pharmacol., **50**, pp. 325–332.
[23] Hirsch, L. R., Stafford, R. J., Bankson, J. A., Sershen, S. R., Rivera, B., Price, R. E., Hazle, J. D., Halas, N. J., and West, J. L., 2003, "Nanoshell-Mediated Near-Infrared Thermal Therapy of Tumors Under Magnetic Resonance Guidance," Proc. Natl. Acad. Sci. USA, **100**(23), pp. 13549–13554.
[24] Qin, Z., and Bischof, J. C., 2010, "One-Dimensional Experimental Setup to Study the Heating of Nanoparticle Laden Systems," Proceedings of the ASME Summer Bioengineering Engineering Conference, Naples, FL, June 16–19, 2010, ASME Paper No. SBC2010-19676.
[25] Elliott, A. M., Stafford, R. J., Schwartz, J., Wang, J., Shetty, A. M., Bourgoyne, C., O'Neal, P., and Hazle, J. D., 2007, "Laser-Induced Thermal Response and Characterization of Nanoparticles for Cancer Treatment Using Magnetic Resonance Thermal Imaging," Med. Phys., **34**, pp. 3102–3108.
[26] Anvari, B., Rastegar, S., and Motamedi, M., 1994, "Modeling of Intraluminal Heating of Biological Tissue: Implications for Treatment of Benign Prostatic Hyperplasia," IEEE Trans. Biomed. Eng., **41**(9), pp. 854–864.
[27] Wang, L., Jacques, S. L., and Zheng, L., 1995, "MCML—Monte Carlo Modeling of Light Transport in Multi-Layered Tissues," Comput. Meth. Prog. Biomed., **47**(2), pp. 131–146.
[28] Wilson, B. C., and Adam, G., 1983, "A Monte Carlo Model for the Absorption and Flux Distributions of Light in Tissue," Med. Phys., **10**(6), pp. 824–830.
[29] Prahl, S. A., Keijzer, M., Jacques, S. L., and Welch, A. J., 1989, "A Monte Carlo Model of Light Propagation in Tissue," SPIE Proc. Dosim. Laser Rad. Med. Biol., **5**, pp. 102–111.
[30] Flock, S. W., Wilson, B. C., and Patterson, M. S., 1989, "Monte Carlo Modeling of Light Propagation in Highly Scattering Tissues-II: Comparison With Measurements in Phantoms," IEEE Trans. Biomed. Eng., **36**(12), pp. 1169–1173.
[31] Keijzer, M., Pickering, J. W., and van Gemert, M. J. C., 1991, "Laser Beam Diameter for Port Wine Stain Treatment Lasers," Laser. Surg. Med., **11**, pp. 601–605.
[32] Keijzer, M., Jacques, S. L., Prahl, S. A., and Welch, A. J., 1989, "Light Distributions in Artery Tissue: Monte Carlo Simulations for Finite-Diameter Laser Beams," Laser. Surg. Med., **9**, pp. 148–154.
[33] Jacques, S., 1989, "Time-Resolved Propagation of Ultra-Short Laser Pulses Within Turbid Tissues," Appl. Opt., **28**, pp. 2223–2229.
[34] Jacques, S., 1989, "Time-Resolved Reflectance Spectroscopy in Turbid Tissues," IEEE Trans. Biomed. Eng., **36**, pp. 1155–1161.
[35] Wang, L., and Jacques, S. L., 1993, "Hybrid Model of Monte Carlo Simulation and Diffusion Theory for Light Reflectance by Turbid Media," J. Opt. Soc., **10**, pp. 1746–1752.
[36] Wang, L., and Jacques, S. L., 1994, "Optimized Radial and Angular Positions in Monte Carlo Modeling," Med. Phys., **21**, pp. 1081–1083.
[37] Wang, L., Jacques, S. L., and Zheng, L. Q., 1997, "CONV—Convolution for Responses to a Finite Diameter Photon Beam Incident on Multi-Layered Tissues," Comput. Meth. Prog. Biomed., **54**, pp. 141–150.
[38] Gardner, C. W., and Welch, A. J., 1994, "Monte Carlo Simulation of Light Transport in Tissue: Unscattered Absorption Events," Appl. Opt., **33**(13), pp. 2743–2745.
[39] Feng, Y. F., Fuentes, D., Hawkins, A., Bass, J., Rylander, M. N., Elliott, A., Shetty, A., Stafford, R. J., and Oden, J. T., 2010, "Nanoshell-Mediated Laser Surgery Simulation for Prostate Cancer Treatment," Eng. Comp., **25**(1), pp. 3–13.
[40] Gardner, C. M., Jacques, S. L., and Welch A. J., 1996, "Light Transport in Tissue: Accurate Expressions for One-Dimensional Fluence Rate and Escape Function Based Upon Monte Carlo Simulation," Laser. Surg. Med., **18**(2), pp. 129–138.
[41] Chen, Y., 2012, "Monte Carlo Simulation of Enhanced Laser Absorption in Tumors With Gold Nano-rod Inclusions: A Study of Laser Thermal Therapy Applied in Tumor Ablation," M.S. thesis, University of Maryland Baltimore County, Baltimore, MD.
[42] Mourant, J. R., Fuselier, T., Boyer, J., Johnson, T. M., and Bigio, I. J., 1997, "Predictions and Measurements of Scattering and Absorption Over Broad Wavelength Ranges in Tissue Phantoms," Appl. Opt., **36**(4), pp. 949–957.
[43] Piao, D. B., Bartels, K. E., Jiang, Z., Holyoak, G. R., Ritchey, J. W., Xu, G., Bunting, C. F., and Slobodov, G., 2010, "Alternative Transrectal Prostate Imaging: A Diffuse Optical Tomography Method," IEEE J. Sel. Topics Quant. Electron., **16**(4), pp. 715–729.

[44] Piao, D. B., Jiang, Z., Bartels, K. E., Holyoak, G. R., Ritchey, J. W., Xu, G., Bunting, C. F., and Slobodov, G., 2009, "In Vivo Trans-Rectal Ultrasound-Coupled Near-Infrared Optical Tomography of Intact Normal Canine Prostate," J. Innovat. Opt. Health Sci., **2**(3), pp. 215–225.
[45] Manuchehrabadi, N. A., Attaluri, A., Cai, H., Edziah, R., Lalanne, E., Bieberich, C., Ma, R., Johnson, A. M., and Zhu, L., 2012, "MicroCT Imaging and In Vivo Temperature Elevations in Implanted Prostatic Tumors in Laser Photothermal Therapy Using Gold Nanorods," ASME J. Nanotech. Eng. Med., **3**(2), p. 021003.
[46] Pennes, H. H., 1948, "Analysis of Tissue and Arterial Blood Temperature in the Resting Human Forearm," J. Appl. Physiol., **1**, pp. 93–122.
[47] Fujita, S. T., Tamazawa, M., and Kuroda, K., 1998, "Effects of Blood Perfusion Rate on the Optimization of RF-Capacitive Hyperthermia," IEEE Trans. Biomed. Eng., **45**(9), pp. 1182–1186.
[48] Gore, J. P., and Xu, L. X., 2003, "Thermal Imaging for Biological and Medical Diagnostics," *Biomedical Photonics Handbook*, T. Vo-Dinh, ed., CRC Press, Boca Raton, FL.
[49] von Maltzahn, G., Park, J. H., Agrawal, A., and Bandaru, N. K., 2009, "Computationally Guided Photothermal Tumor Therapy Using Long-Circulating Gold Nanorod Antennas," Cancer Res. Suppl. Data, **69**(9), pp. 3892–3900.
[50] Manuchehrabadi, N., Attaluri, A., Cai, H., Edziah, R., Lalanne, E., Bieberich, C., Ma, R., Johnson, A. M., and Zhu, L., 2013, "Tumor Shrinkage Studies and Histological Analyses after Laser Photothermal Therapy Using Gold Nanorods," International Journal of Biomedical Engineering and Technology, **12**(2), pp. 157–174.
[51] Jain, P. K., Lee, K. S., El-Sayed, I. H., and El-Sayed M. A., 2006, "Calculated Absorption and Scattering Properties of Gold Nanoparticles of Different Size, Shape, and Composition: Applications in Biological Imaging and Biomedicine," J. Phys. Chem., 110, pp. 7238–7248.
[52] Arnifield, M. R., Mathew, R. P., Tulip, J., and Mcphee, M. S., 1992, "Analysis of Tissue Optical Coefficients Using an Approximate Equation Valid for Comparable Absorption and Scattering," Phys. Med. Biol., 37, pp. 1219–1230.
[53] Song, C. W., 1984, "Effect of Local Hyperthermia on Blood Flow and Microenvironment: A Review," Cancer Res., 44, pp. 4721s–4730s.
[54] Zhu, L., 2009, "Heat Transfer Applications in Biological Systems.," *Biomedical Engineering & Design Handbook*, *Volume 1: Bioengineering Fundamentals*, M. Kutz, editor-in-chief, McGraw-Hill, New York, pp. 2.33–2.67.
[55] Moritz, A. R., and Henriques, F. C. 1947, "The Relative Importance of Time and Surface Temperature in the Causation of Cutaneous Burns," Am. J. Pathol., 23, pp. 695–720.